INTEGRATED MODELING AND CONTROL OF FLEXIBLE AIRCRAFT WINGS

Ву

Dagmara Anna Wehr

A THESIS

Submitted to
Michigan State University
in partial fulfillment of the requirements
for the degree of

Electrical Engineering – Master of Science

2014

ABSTRACT

INTEGRATED MODELING AND CONTROL OF FLEXIBLE AIRCRAFT WINGS

By

Dagmara Anna Wehr

Structural control for vibration reduction has important applications in many research areas, including the effect of earthquakes on buildings and aerodynamic forces on aircraft stability and performance. Both passive and active control techniques have been implemented, with the best solution usually involving a passive approach followed by an active one. This thesis presents an integrated modeling and controller design approach. Modal Cost Analysis (MCA) and Output Covariance Constraint (OCC) control are used to reduce a high-order aeroelastic wing model to establish the best controller for the reduced-order model, with a constraint on the covariance of the vibration outputs. MCA seeks to keep the modes that have the highest contribution to a given cost function. Using iterations on the two processes will allow a lower-order controller to be designed and result in the same performance.

The OCC and MCA methods and their respective algorithms are presented, and an approach to integrate the two procedures is given. NASA's model used in this thesis is applied to the MCA and OCC algorithms using MATLAB. A 40th-order wing model is derived. The model reduction technique initially reduces the system to a 12th order one. A simulation of the OCC algorithm is performed on the reduced-order model and applied to the full-order model. The controller resulting in the best closed-loop performance is shown to significantly reduce the vibrations due to wind. A corresponding weighting matrix used in OCC is then used for a second round of MCA to further reduce the model to an 8th order model. A lower-order controller designed for this second model is shown to similarly reduce the output vibrations.

ACKNOWLEDGEMENTS

Over the past two years, I have received support and encouragement from a number of individuals. First, I would like to thank my advisor, Dr. Guoming (George) Zhu for his guidance and support in my research and thesis. His guidance made this a thoughtful, manageable effort. I would also like to thank Dr. Xiaobo Tan and Dr. Hassan Khalil for serving on my guidance committee.

I would also like to thank Dr. Percy Pierre and Dr. Xiaobo Tan for their support in helping me attend and be successful in my graduate studies.

Finally, I would like to thank my family for their support. They believed in me and made me believe in myself during rough periods.

TABLE OF CONTENTS

LIST OF TABLES	v
LIST OF FIGURES	vi
CHAPTER 1: INTRODUCTION	1
1.1 Structural Control for Vibration Reduction	
1.1.1 Passive Control	
1.1.2 Active Control	
1.1.3 Combining Passive and Active Control	
1.2 Related Research	
1.2.1 Related Applications	
1.2.2 Model Reduction Methods	
1.3 Objective and Problem Statement	
1.4 Thesis Outline	
CHAPTER 2: REVIEW OF METHODS	11
2.1 Output Covariance Constraint (OCC) Control	
2.1.1 Output Covariance Constraint Control Problem	
2.1.2 OCC Algorithm	
2.2 Model Reduction Using Modal Cost Analysis	
2.3 Integration of Controller Design and Model Reduction	
CHAPTER 3: AIRCRAFT WING MODEL AND SIMULATION	17
3.1 Modeling Description	17
3.2 Model Reduction	20
3.3 Simulation Study	22
3.3.1 Simulation Set-Up	22
3.3.2 Simulation Results	24
3.3.3 Iteration on OCC and MCA	28
CHAPTER 4: CONCLUSION	35
APPENDIX	36
RIBI IOGRAPHY	40

LIST OF TABLES

Table 3.1.	Modal Cost Analysis	21
	•	
Table 3.2.	Modal Cost Analysis for Q Loop 1	30

LIST OF FIGURES

Figure 2.1.	Q Loop Diagram	16
Figure 3.1.	Locations of Measured and Control Outputs	20
Figure 3.2a.	Impulse Response of Evaluation and Design Models: 6 th Input to 4 th Output	22
Figure 3.2b.	Impulse Response of Evaluation and Design Models: 6 th Input to 5 th Output	22
Figure 3.3.	Output Variance vs. Iteration Number	25
Figure 3.4.	Output Variance vs. Input Covariance	26
Figure 3.5a.	Impulse Response of the Open and Closed-Loop Systems from Wind Input to 5 th Output	26
Figure 3.5b.	Impulse Response of the Open and Closed-Loop Systems from Wind Input to 7 th Output	27
Figure 3.6a.	Open-Loop Wing Deformation with Time	28
Figure 3.6b.	Closed-Loop Wing Deformation with Time	28
Figure 3.7a.	Impulse Response of Evaluation and 8 th Order Design Models: 6 th Input to 4 th Output	30
Figure 3.7b.	Impulse Response of Evaluation and 8 th Order Design Models: 4 th Input to 5 th Output	31
Figure 3.8a.	Output Variance vs. Iteration Number for Q Loop 1	32
Figure 3.8b.	Output Variance vs. Input Covariance for Q Loop 1	32
Figure 3.9a.	Open vs. Closed-Loop Impulse Response of Wind to 5 th Output for Q Loop 1	33
Figure 3.9b.	Open vs. Closed-Loop Impulse Response of Wind to 7 th Output for Q Loop 1	33
Figure 3.10.	Closed-Loop Wing Deformation with Time for Q Loop 1	34

CHAPTER 1: INTRODUCTION

1.1 Structural Control for Vibration Reduction

Structural control for vibration reduction has been employed in various fields including civil and aerospace structures to protect against the possibly devastating effects of vibrations caused by natural forces such as wind and earthquakes. With the invention of structures with newer designs, using modern materials and shapes, comes the increased need for methods that reduce vibrations caused by environmental or other forces. To achieve this, the control design should consider both passive and active control. The following sections discuss different types of control, as well as their traditional and recent applications.

1.1.1 Passive Control

Passive control can refer to two kinds of vibration suppression. One describes passive actuators, traditionally used in building designs, and the other to "structural redesign", in which system parameters, such as those corresponding to damping, are modified to improve performance [1], [2].

In the first case, passive control describes the use of devices that do not use external energy sources to reduce vibrations of structures. As opposed to active controllers, they reduce vibrations without any sensors or feedback. Passive controllers, such as tuned liquid dampers and tuned mass dampers (TMDs), have been widely used for civil engineering applications, especially as a means to counteract the effects of earthquakes. These devices have the ability to control high-amplitude forces reliably and cost-effectively [1]. Purely passive TMDs, also referred to as tuned vibration absorbers (TVAs), have been applied to tall buildings, bridges, offshore platforms, and pipelines, each of which experience one of more forces from winds,

earthquakes, or sea waves. Aerospace applications include helicopter rotor hubs, and noise radiation from structural resonance vibrations such as cabin noise [3]. [4] also discusses passive control methods for various sources of aircraft vibration suppression. The author presents a method consisting of "fuselage double-partition constructions with acoustic insulation coating" for noise vibration reduction. He also describes actuators mounted on the fuselage skin or frame to minimize vibrations [4].

In the second definition of passive control, system redesign is used in structures as a means to minimize the active control needed [2]. Therefore, it involves system design rather than direct control techniques. Often, changes to the plant can improve the system's performance beyond what can be achieved by feedback control, and these changes can be implemented more easily than designing a new controller. Plant and controller design are a related process, because controllers are designed to modify the dynamics of a system which could otherwise be modified by a change in plant parameters [2]. For this reason, [2] proposes an iterative technique to simultaneously design the plant and controller. When the plant and controller are redesigned in subsequent iterations, the goal is to maintain the desired performance while minimizing the control energy [2]. This structural redesign approach is also applied in [5] to a cantilever beam as a means to control vibrations of structures that resemble cantilevers.

1.1.2 Active Control

Active control is often necessary and allows going beyond passive control by efficiently applying an appropriate control force at each moment to counteract structural vibrations, using sensors and actuators. This type of control allows moderating multiple vibration modes at once with one device. So, it is an effective method for controlling structures with several vibration modes that contribute to unwanted structural dynamics. Furthermore, active controllers are

versatile and can be completely stable if collocated control is used. However, active control techniques are expensive, as a result of a higher level of technology and required maintenance. Additionally, often large control devices and power supply systems are needed [1]. Reliability problems arise in civil structures if the power to a building is cut, which is possible during an earthquake [6].

The use of active mass dampers for buildings is mentioned in [7]. [1] also applies active controllers in the form of active mass dampers to a 3 story building model and a real footbridge, as well as an active bracing system to the building model. Applications of active TMDs can include classical control, fuzzy logic, and neural networks [3]. Active control in the form of active velocity feedback is demonstrated for a cantilever beam in [8] to reduce its first 3 vibration modes. [9] describes the use of active control to reduce structural vibrations in a blended wing-body type aircraft for ride comfort and improved handling qualities.

1.1.3 Combining Passive and Active Control

Due to the advantages and disadvantages of both passive and active controllers, the two techniques are often combined in the form of structural redesign (Section 1.1.1), semi-active control, or hybrid control. Use of passive techniques is frequently used to supplement the necessity of active controllers. Therefore, when considering control techniques, passive control should be considered first, then improved upon using active control approaches.

In an aircraft, aeroelasticity is determined by the aircraft's structural, damping, and mass characteristics, not only by the external forces. Therefore, considering passive control in the sense of model redesign is extremely beneficial. This way, an efficient and simpler active controller can be designed to an already properly-damped system. Since plant and controller design problems are not independent, basic changes in the plant can also often result in great

improvements in performance and robustness over just using feedback control [2]. In [2], an iterative technique for plant and controller redesign is proposed to make control of the system easier.

Semi-active control refers to using a passive device that can be controlled actively [6]. Semi-active, sometimes called adaptive, control devices have advantages over fully active systems. Passive controllers have their advantages, but can lose their effectiveness over time. It is therefore useful to be able to modify, or adapt, these devices actively to changing operating and environmental conditions. The disadvantage of semi-active systems lies in their many components which may need continual maintenance [3]. The use of semi-active TMDs is mentioned for several applications in [3]. Semi-active control is also studied in the context of building vibration control as a solution that offers higher energy-efficiency than active devices and is more effective at reducing seismic vibrations than passive devices [10]. In [10], a controller is developed to adjust the damping of a type of semi-active control called a magnetorheological damper, which changes its damping based on changing the viscosity of a fluid using a magnetic field. [6] also mentions the use of semi-active control in the form of hydraulic dampers, fluid viscous dampers, variable-orifice dampers, variable-friction dampers, electrorheological, and magetorheological devices. The main advantage of semi-active controllers is that they run on battery power and are not destabilizing [6]. [7] mentions the use of a semi-active hydraulic damper on a bridge.

Both [6] and [7] discuss hybrid control, such as a hybrid mass damper in [8], which uses a combination of passive actuators and active control devices. Since a passive device is used, less control energy is needed for the active component. Along with semi-active control, hybrid control techniques are more reliable against power failures, as they can support some level of

damage prevention over purely active control systems in this case [7]. Many active TMDs are actually hybrid, consisting of passive devices as well. In the context of a building, the active device would be used for small vibrations due to wind, and passive for stronger reactions caused by earthquakes [3].

1.2 Related Research

1.2.1 Related Applications

This research is closely based on the work in [11]. In [11], the authors simultaneously consider modeling and controller design of flexible aircraft wings. Modal Cost Analysis (MCA) is used to reduce the high-order finite-dimension state-space model for a desired output covariance, with the output consisting of displacement and rates of points on the wing. A reduced-order model is used to design a dynamic output feedback controller using Output Covariance Constraint (OCC) control. The controller is then evaluated with the full-order model to confirm handling performance requirements have been met, and the wing fluttering motion has been almost completely eliminated [11].

Active flutter suppression of the NASA Benchmark Active Controls Technology (BACT) wing using a gain-scheduled controller utilizing a linear fractional transformation is studied in [12]. The goal of [12] is to increase disturbance rejection and the stable operating range. Since the wing section varies with Mach and dynamic pressure changes, the controller is made as a function of the two changing dynamics. As a comparison, a linear controller is also designed using D-K iteration. The performance is analyzed with maximum singular value plots and time simulations. The gain-scheduled controller is found to be stable over the specified operating range, and have significant performance improvement [12].

Generalized Predictive Control (GPC) for a wind-tunnel wing model for flutter

suppression is presented in [13]. The control technique minimizes a cost function consisting of the sum of the mean square output and the square rate of change of the control input. The algorithm uses the model output to predict an arbitrary input's effect on plant dynamics. A BACT plant is reduced using an auto-regressive moving-average model. The cost function is modified to account for the output being invariant to low-frequency inputs caused by a drift in the control input. Simulations including the wind-tunnel test confirm flutter suppression robust to a wide range of conditions and modeling errors [13].

1.2.2 Model Reduction Methods

There are several model reduction techniques that have been developed for largedimensioned systems. In [14], the author mentions several such methods appropriate to his application of large space structures including the Internal Balancing Method, Component Cost Analysis (CCA), Modal Cost Analysis (MCA), and the Canonical Correlation Analysis Method. The Internal Balancing Method is based on measures of controllability and observability, removing the least controllable and least observable parts to form a reduced-order model. CCA and MCA (which is a special case of CCA), and their variations, Weighted Component Cost Analysis (WCCA) and Weighted Modal Cost Analysis (WMCA), take into account the system's different components to reduce them separately. CCA considers any system as made up of components, and reduces it based on the different components' contributions to some quadratic cost functional. MCA is a special case of CCA, which uses the system described by its modes. The weighted versions of these two methods are used when input dynamics are considered, instead of just white noise input. The Canonical Correlation Analysis Method also uses a system's components, as well as their interactions, to rank the components by their canonical correlation coefficients and delete the smallest ones to form the reduced-order model [14]. The

methods applied in [14] are WMCA and a combination of CCA with Canonical Correlation Analysis. MCA is also used in [15] and [16] for aerospace applications.

Several other model reduction methods are considered in [6] and [17], which are divided into three types: nodal truncation, singular value decomposition (SVD)-based methods, and Krylov-based methods. Nodal truncation algorithms, including Guyan reduction, truncates nodes (from finite element methods) based on their influence on the structure's mass and stiffness matrices. The standard approach used in industry for civil structure applications is modal truncation, since higher modes usually have less influence on the system response than lower modes. However, this method has high computational costs. The SVD-based methods, including balanced model reduction, rely on the system's Hankel singular values and balancing of the system to determine the contribution of each state. However, this method is computationally demanding for large-scale systems. Finally, the Krylov methods rely on moment matching to iteratively match moments of original and lower-order models [6]. [6] presents these methods in the context of civil structure modeling and control, and [17] mentions an application to the International Space Station.

1.3 Objective and Problem Statement

With the development of modern materials, their use in new airplane wing designs has been studied in recent years [11], [18]. Using materials that are more lightweight and flexible leads to more energy-efficient aerodynamic designs, improving cruise efficiency and lowering drag [11]–[13], [18]. Materials such as composites are less rigid than in previous-generation designs, while preserving the necessary load-carrying capacity. The Boeing 787 Dreamliner aircraft is an example of the highly-flexible wing structure. The concept is that the flexible wing surfaces are shaped during flight to change the angle of attack in a way that drag can be reduced,

resulting in lower fuel burn during cruise [18]. With increased structural flexibility, however, come increased effects of aerodynamic forces on the aircraft's stability and performance [11].

The objective of this work was to combine model reduction and controller design to actively suppress the wing vibrations of a NASA aircraft model. Model reduction and controller design was done together and iteratively to produce the best controller for the reduced-order model, and again, the best reduced model for the chosen controller. Output Covariance Constraint (OCC) control was used for controller design, and Modal Cost Analysis (MCA) was used for model reduction. It was expected that the controller designed using OCC for the design model could significantly reduce the wing vibrations due to a random wind input. In addition, through an iteration of model reduction and controller design, the closed-loop performance could be matched with a lower-order controller than the initial reduced-order model.

MCA and OCC was an appropriate choice of model reduction and controller design methods due to their interaction, to achieve the goal of better performance by coupling the two design steps. MCA is effective for reducing large models that can be expressed by a sum of their vibration modes. In MCA, a cost is found for each mode to an output covariance cost function, and the lowest-cost modes are truncated. The performance requirements for aeroelastic aircraft wings vibrating due to wind can also be expressed in terms of output covariance [11]. A physical interpretation of OCC can be given by a bound on the peak magnitude of the time response [15]. If the output covariance constraint is expressed by σ , and if there is a constraint

$$\mathcal{E}_{\infty}(yy^T) \leq \sigma$$
,

then the peak magnitude of the time response of the output $||y||_{\infty}$ in the presence of bounded energy disturbances, w_p and v, is bounded such that [15]:

$$||y||_{\infty}^2 \le \sigma ||w_p^T v^T||_2^2.$$

The OCC problem seeks to find a proper weighting matrix that leads to a controller which minimizes the control effort while meeting constraints on output covariance [11]. This weighting matrix is in turn used in MCA.

The work of this thesis is based on [11], which uses MCA and OCC to control vibrations of a flexible wing structure. However, it goes a step further by iterating on the model reduction and controller design steps for a second time, as mentioned previously. By choosing an appropriate weighting matrix found in the first iteration of the OCC control design, this weighting is used to better determine the significant modes that contribute to the output. This allows an even lower-order controller to be designed with very similar performance.

1.4 Thesis Outline

The rest of this thesis consists of three chapters. In Chapter 2, the methods used in the research are presented. First, the definition and algorithm of the OCC problem is presented. Next, MCA is discussed as a method for model reduction. Finally, the importance of coupling model reduction and controller design is discussed.

Chapter 3 presents the application, mentioned above, of the methods given in Chapter 2. The model of the aircraft is derived and the simulation parameters are given. Next, details of how the reduced model was found using MCA is presented. A comparison of the full-order and reduced-order model is shown with their impulse responses. Section 3.3 summarizes the steps taken to carry out the OCC control design algorithm with the reduced-order model. The output variances are plotted against the trace of the input (control) covariance, and a time response comparing open and closed-loop systems is presented. Afterward, the iteration on MCA and OCC is given, and the model is taken through a second round of model reduction and controller design. Similar plots as in the first iteration are shown.

The third and final chapter presents the conclusions.

CHAPTER 2: REVIEW OF METHODS

2.1 **Output Covariance Constraint (OCC) Control**

2.1.1 **Output Covariance Constraint Control Problem**

Consider a continuous linear time-invariant system,

$$\dot{x}_p = A_p x_p + B_p u + D_p w_p \tag{2.1a}$$

$$y_p = C_p x_p$$
 (2.1b)

$$z = M_p x_p + v,$$
 (2.1c)

$$z = M_p x_p + v, (2.1c)$$

with white noise signals w_p and v of intensities W and V, respectively, and a strictly proper fullorder dynamic controller,

$$\dot{x}_c = A_c x_c + Fz \tag{2.2a}$$

$$u = G x_c \tag{2.2b}$$

$$u = Gx_c. (2.2b)$$

The closed-loop system that results from applying the controller (2.2) to the plant (2.1) is

$$\dot{x} = Ax + D\overline{w} \tag{2.3a}$$

$$y = Cx, (2.3b)$$

where

$$x = \begin{bmatrix} x_p \\ x_c \end{bmatrix} \tag{2.4a}$$

$$\overline{w} = \begin{bmatrix} w_p \\ v \end{bmatrix} \tag{2.4b}$$

$$y = y_p. (2.4c)$$

Substituting Equations (2.1) and (2.2) into (2.3), Equation (2.3) can be expressed as:

$$\begin{bmatrix} \dot{x}_p \\ \dot{x}_c \end{bmatrix} = \begin{bmatrix} A_p & B_p G \\ FM_p & A_c \end{bmatrix} \begin{bmatrix} x_p \\ x_c \end{bmatrix} + \begin{bmatrix} D_p & 0 \\ 0 & F \end{bmatrix} \begin{bmatrix} w_p \\ v \end{bmatrix}$$
 (2.5a)

$$y = \begin{bmatrix} C_p & 0 \end{bmatrix} \begin{bmatrix} x_p \\ x_c \end{bmatrix}; u = C_u = \begin{bmatrix} 0 & G \end{bmatrix} \begin{bmatrix} x_p \\ x_c \end{bmatrix}.$$
 (2.5b)

Then, let

$$\overline{W} = \begin{bmatrix} W & 0 \\ 0 & V \end{bmatrix}. \tag{2.6}$$

If \hat{X} represents the closed-loop controllability Gramian from the disturbance input \overline{w} , then \hat{X} satisfies

$$0 = A\hat{X} + \hat{X}A^T + DWD^T. \tag{2.7}$$

The following is the definition for the Output Covariance Constraint (OCC) problem: Find a controller to minimize the cost function,

$$J = trace\{RC_{\nu}\hat{X}C_{\nu}\}, \tag{2.8}$$

where R > 0 is a diagonal weighting matrix, subject to the system Equations (2.1) to (2.5) above, and

$$Y_i = C_i \hat{X} C_i^T \le \bar{Y}_i^b$$
, $i = 1, 2, ..., m$, (2.9)

where m is the dimension of the output y, $\bar{Y}_i^b > 0$ $(i=1,2,...,m), C^T = [C_1^T, C_2^T,..., C_m^T]$, and $\overline{Y}^b = block \ diag[\overline{Y}_1^b, \overline{Y}_2^b, \dots, \overline{Y}_m^b].$ This means that the OCC problem is to minimize the weighted control energy with certain constraints on the block diagonal matrix $Y = block \ diag[Y_1, Y_2, ..., Y_m]$ consisting of the output variances [19], [20].

Suppose that (A_c, F, G) is an optimal solution to the OCC problem. Then there exists a semi-definite matrix,

$$Q = block \ diag[Q_1, Q_2, ..., Q_m] \ge 0 \ , i = 1, 2, ..., m, \tag{2.10}$$

such that

$$A_c = A_p + B_p G - F M_p \tag{2.11a}$$

$$A_c = A_p + B_p G - F M_p$$
 (2.11a)
 $G = -R^{-1} B_p^T K$ (2.11b)
 $F = \widetilde{X} M_p^T V^{-1}$ (2.11c)

$$F = \widetilde{X} M_p^T V^{-1} \tag{2.11c}$$

$$0 = A_p^T K + K A_p - K B_p R^{-1} B_p^T K + C_p^T Q C_p$$
 (2.11d)

$$0 = A_n \widetilde{\mathbf{X}} + \widetilde{\mathbf{X}} A_n^T - \widetilde{\mathbf{X}} M_n^T V^{-1} M_n \widetilde{\mathbf{X}} + D_n W_n D_n^T$$
 (2.11e)

$$0 = A_{p}\widetilde{X} + \widetilde{X}A_{p}^{T} - \widetilde{X}M_{p}^{T}V^{-1}M_{p}\widetilde{X} + D_{p}W_{p}D_{p}^{T}$$

$$0 = (A_{p} + B_{p}G)X + X(A_{p} + B_{p}G)^{T} + FVF^{T}$$

$$0 = (Y_{i} - \overline{Y}_{i})Q_{i} ; Y = C_{p}(X + \widetilde{X})C_{p}^{T},$$
(2.11e)
(2.11f)

$$0 = (Y_i - \bar{Y}_i)Q_i \; ; \; Y = C_n(X + \tilde{X})C_n^T , \qquad (2.11g)$$

where $\hat{X} = block \ diag \ [X + \widetilde{X}, \widetilde{X}]$ is the closed-loop covariance of x and Y is the covariance of

output y [19], [20].

2.1.2 OCC Algorithm

An algorithm for finding the optimal solution of the OCC problem discussed above is described as follows [19], [20]:

Given $A_p, B_p, C_p, D_p, W_p, R, \overline{Y}^b$, initial Q(0), and tuned parameters $\alpha > 0$ and $0 < \beta < 1$, let j = 0 and proceed to 1).

- 1) Compute F and \tilde{X} by solving (2.11c) and (2.11e).
- 2) Compute K(j) and G(j) by solving

$$0 = A_p^T K(j) + K(j) A_p - K(j) B_p R^{-1} B_p^T K(j) + C_p^T Q(j) C_p$$

$$G(j) = -R^{-1} B_p^T K(j).$$
(2.12)
(2.13)

$$G(j) = -R^{-1}B_p^T K(j). (2.13)$$

3) Compute X(j) by solving

$$0 = [A_p + B_p G(j)]X(j) + X(j)[A_p + B_p G(j)]^T + FVF^T.$$
(2.14)

- 4) Compute $Y_i(j) = C_i(\tilde{X} + X)C_i^T$, i = 1, 2, ..., m.
- 5) Let $Y^{b}(j) = block \ diag \ [Y_{1}(j), Y_{2}(j), ..., Y_{m}(j)]$ and

$$Q(j+1) = \beta Q(j) + (1-\beta)\mathcal{P}[Q(j) + \alpha \{Y^b(j) - \overline{Y}^b\}].$$
 \mathcal{P} is defined below.

If $\|(Y^b(j) - \overline{Y}^b)Q(j)\| < \varepsilon$, where ε is some specified tolerance, stop. Otherwise, go back to step 2 with j = j + 1.

When the algorithm above ends, the dynamic controller

$$\dot{x}_c = (A_p + B_p G - F M_p) x_c + F z \tag{2.15a}$$

$$u = Gx_c, (2.15b)$$

is an optimal solution to the OCC problem [19], [20].

The operator \mathcal{P} used in step 5 of the algorithm above is defined in the following way [15]: Let M represent a real, symmetric matrix that can be written in the Schur decomposition form as follows:

$$M = \begin{bmatrix} U_1 & U_2 \end{bmatrix} block \ diag \begin{bmatrix} E_p & E_n \end{bmatrix} \begin{bmatrix} U_1 \\ U_2 \end{bmatrix}, \tag{2.16}$$

where E_p and E_n are diagonal and consist of the positive and non-positive eigenvalues of M, respectively, and $\begin{bmatrix} U_1 \\ U_2 \end{bmatrix}$ is a unitary orthogonal matrix. Then,

$$\mathcal{P}[M] = \begin{cases} 0 & if \ M \le 0 \\ U_1 E_p U_1^T & otherwise \end{cases}$$
 (2.17)

A MATLAB program used in Section 3.3 for the simulation implementing the OCC algorithm is given in the Appendix.

2.2 Model Reduction Using Modal Cost Analysis

There are several ways to design a reduced-order controller for a high-order system, for which a full-order controller has implementation limitations due to a computational limitation of the real-time microcontroller. One method is to directly design a fixed-order controller. Another approach is to design a full-order controller and then conduct a controller order reduction to get the reduced-order controller. Lastly, the method used in this thesis is to first reduce the system model, and then design a full-order controller for the reduced model [16]. One advantage of using this approach is that the designed reduced-order control at least stabilizes the reduced-order model. However, the quality of the reduced-order controller is heavily dependent on the accuracy of the model reduction. One such model-reduction approach presented here, Modal Cost Analysis (MCA), can be used to reduce a high-order system model, especially for a structure system model, when it is expressed in its modal coordinates. MCA takes into account the modes of the system, finding and truncating those modes that have the lowest contribution to the output. This method calculates each modal contribution, v_i , to the weighted cost function

$$v \triangleq \mathcal{E}_{\infty} \{ y^T Q y \} = \sum_{i=1}^N v_i , \qquad (2.18)$$

where \mathcal{E}_{∞} is the expectation operator, y is the output vector, N is the number of modes in the

system, and Q is the weighting matrix for modal cost analysis which could be from Equation (2.10) [15]. The function corresponds to the weighted output variance with respect to the white noise input [16].

Recall the system Equations (2.1). If the state-space parameters were transformed into their modal coordinates, \hat{A} , \hat{B} , \hat{C} , \hat{D} , \hat{M} , then the Lyapunov equation,

$$0 = \hat{A}\hat{X} + \hat{X}\hat{A}^T + \hat{D}W\hat{D}^T, \tag{2.19}$$

gives the solution \hat{X} , where W is as in Equation (2.6). Then, the modal costs can be calculated by

$$v_i = trace[\hat{C}^T Q \hat{C} \hat{X}]_{ii}, i = 1, 2, ..., N$$
 (2.20)

where *N* is the number of modes. The resulting modes can be ranked as

$$|v_1| \ge |v_2| \ge \cdots \ge |v_N|$$
,

where v_1 now corresponds to the highest modal cost, not necessarily to the first mode. The modes corresponding to the lowest modal costs v_i are then truncated to give a lower-order model [11].

2.3 Integration of Controller Design and Model Reduction

When designing a controller for a reduced-order model, model reduction and controller design is an integrated process. Using this method of designing a controller for a reduced-order model, the neglected dynamics of the system will have an effect on how well the controller works with the actual, full-order model [16]. Since the controller designed for the reduced model may not be the best for the full-order model that it has to control, an iterative approach is used in [15], [16] with an application to space structures. During this process, the best controller is designed for a reduced-order model, after which the model reduction process is repeated to produce the best model for the current controller [16].

The weighting matrix Q introduced in Equation (2.10) of section 2.1.1 is the same one used in both MCA and the beginning of OCC. Q is a diagonal matrix, with relative higher-valued elements emphasizing certain system outputs. In this way, the choice of Q affects the modal costs, and therefore the resulting model reduction. Q also affects the output variance calculations. Combining the model reduction and controller design processes allows Q to represent the most significant outputs and retain the most significant modes [11].

A diagram of what will be referred to as the Q Loop in Chapter 3 is presented in Figure 2.1. As the figure shows, the chosen Q from the OCC controller design is used in another iteration of model reduction using MCA.

A software package in MATLAB including the algorithms for the integration of model reduction and controller design are used in [15], [16] and is described in [21].

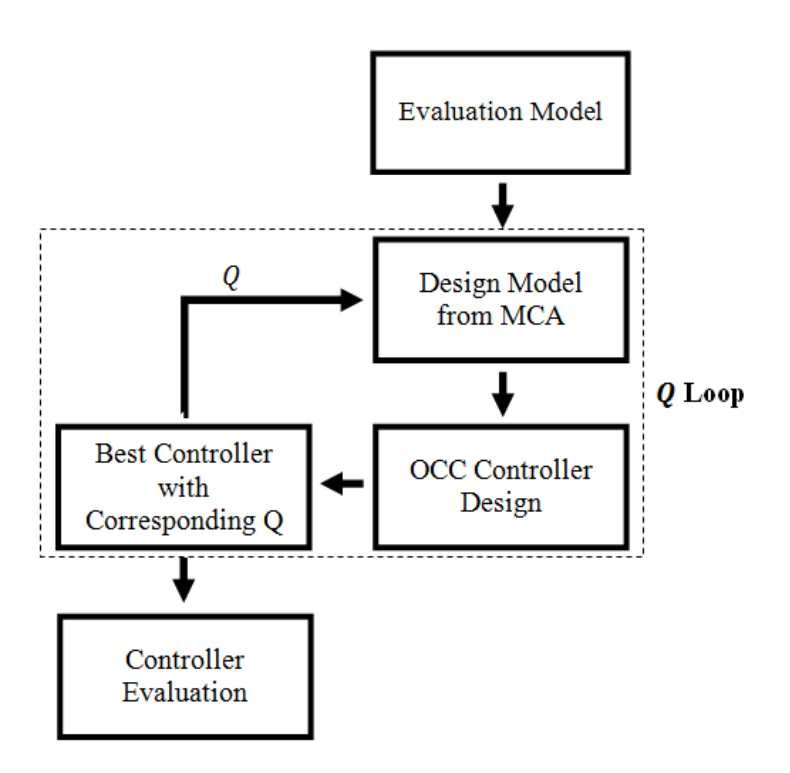


Figure 2.1. Q Loop Diagram

CHAPTER 3: AIRCRAFT WING MODEL AND SIMULATION

3.1 Modeling Description

The aircraft wing model is described in [11] by combining the aeroelastic and rigid body aircraft dynamics with wind turbulence and actuator dynamics. The aircraft dynamics are described by the following equations:

$$M_e \ddot{x}_e + C_e \dot{x}_e + K_e x_e + C_a x_a = \left[D_f D_s \right] \begin{bmatrix} \delta_f \\ \delta_s \end{bmatrix}$$
 (3.1a)

$$\dot{x}_a = A_a x_a + A_s x_e + A_d \dot{x}_e + B_e \delta_e + \left[B_f B_s \right] \begin{bmatrix} \delta_f \\ \delta_s \end{bmatrix}, \tag{3.1b}$$

where $x_e = [w_1 w_2 \cdots w_{10} \ \theta_1 \theta_2 \cdots \ \theta_{10}]^T$ are the bending and torsional displacements of the 20 aeroelastic modes, $x_a = [a \ q]^T$ are the rigid body states (angle of attack and pitch rate), δ_e is the elevator deflection angle, δ_f is the flap deflection, and δ_s is the slat deflection. Equation (3.1) can be written in state-space form as follows:

$$\dot{x}_p = A_p x_p + B_p u_\delta \tag{3.2}$$

where $x_p = [x_e \ \dot{x}_e \ x_a]^T$, $u_{\delta} = [\delta_e \ \delta_f \ \delta_s]^T$,

$$A_{p} = \begin{bmatrix} 0 & I & 0 \\ -M_{e}^{-1}K_{e} & -M_{e}^{-1}C_{e} & -M_{e}^{-1}C_{a} \\ A_{s} & A_{d} & A_{a} \end{bmatrix}$$
(3.3a)

$$B_p = \begin{bmatrix} 0 & 0 & 0 \\ 0 & M_e^{-1} D_f & M_e^{-1} D_s \\ B_e & B_f & B_s \end{bmatrix}.$$
 (3.3b)

A turbulence model is then added to the above to include the effect of random wind gust dynamics. It is assumed to be in the following form:

$$\dot{x}_w = A_w x_w + B_w w_a \tag{3.4a}$$

$$y_w = C_w x_w + D_w w_q, (3.4b)$$

with states x_w , random wind gust w_g modeled by zero-mean white noise with intensity W, and

 y_w the total random wind input to the wing model. Combining the turbulence model with the wing dynamics model gives the following representation:

$$\dot{x}_p = A_p x_p + B_p u_\delta + y_w. \tag{3.5}$$

The input u_{δ} that comes from the actuators follows a system:

$$\dot{x}_{\delta} = A_{\delta} x_{\delta} + B_{\delta} u \tag{3.6a}$$

$$u_{\delta} = C_{\delta} x_{\delta} \,, \tag{3.6b}$$

with states x_{δ} and control command u.

To obtain the complete open-loop state-space system, Equations (3.4-3.6) are combined to give

$$\dot{x} = Ax + Bu + Dw, \tag{3.7}$$

where $x = [x_p \ x_w \ x_\delta],$

$$A = \begin{bmatrix} A_p & C_w & B_p C_{\delta} \\ 0 & A_w & 0 \\ 0 & 0 & A_{\delta} \end{bmatrix}$$
 (3.8a)

$$B = \begin{bmatrix} 0 \\ 0 \\ B_{\delta} \end{bmatrix} \tag{3.8b}$$

$$D = \begin{bmatrix} D_w & B_p \\ B_w & 0 \\ 0 & 0 \end{bmatrix}. \tag{3.8c}$$

Then, the performance outputs y and measurement outputs z are given by

$$y = Cx \tag{3.9a}$$

$$z = Mx + v \,, \tag{3.9b}$$

where v is the zero-mean white noise of the sensors, with intensity V. Combining the previous two equations with Equation (3.7) gives the open-loop state-space representation of the whole, full-order system, which was provided by NASA. This system will be referred to as the evaluation model:

$$\dot{x} = Ax + Bu + Dw \tag{3.10a}$$

$$y = Cx \tag{3.10b}$$

$$z = Mx + v \tag{3.10c}$$

where $x \in \mathbb{R}^{45}$, $u \in \mathbb{R}^{13}$, $w \in \mathbb{R}$, $y \in \mathbb{R}^{12}$, $z \in \mathbb{R}^{42}$, and

 $x = [a \ q \ w_1 \cdots w_{10} \ \theta_1 \cdots \theta_{10} \dot{w_1} \cdots \dot{w}_{10} \ \dot{\theta_1} \cdots \dot{\theta}_{10} \ x_w]^T$. The first two states of x represent angle of attack and pitch rate, the next 20 states the 10 bending and 10 torsional states, the following 20 states the rates of the 10 bending and 10 torsional states, and lastly the 3 turbulence states. However, to simplify the simulation, the rigid body mode and turbulence states were removed after transforming the model to its modal coordinates (discussed in Section 3.2), leaving only the 40 aeroelastic states. This simplified model assumes all forces are applied to the wings.

After simplification, the control outputs are $y = [b_1 \cdots b_5 \ t_1 \cdots t_5]$ where $b_1 \cdots b_5$ are bending displacement measurements (in feet) at 5 locations and $t_1 \cdots t_5$ are the torsional displacement measurements (in radians) at those locations. The measurement outputs $z = [b_1 \cdots b_{10} \ t_1 \cdots t_{10} \ \dot{b}_1 \cdots \dot{b}_{10} \ \dot{t}_1 \cdots \dot{t}_{10}]$ are the bending and torsional deflections along with their corresponding rates at 10 locations. Figure 3.1 below, provided by NASA, shows the locations of the measurements and control outputs – 10 equally spaced points along the wing with the last one being on the wingtip for the measurements, and the last 5 of these coinciding with the control outputs [11]. The controls include an elevator, 6 flaps, and 6 slats. The random wind gust w is ± 20 ft/s, which gives $W = 20^2 = 400$. v is the random measurement noise, chosen as 5% of w. Therefore, $V = (0.05 \cdot 20)^2 = 1$ for each measurement.

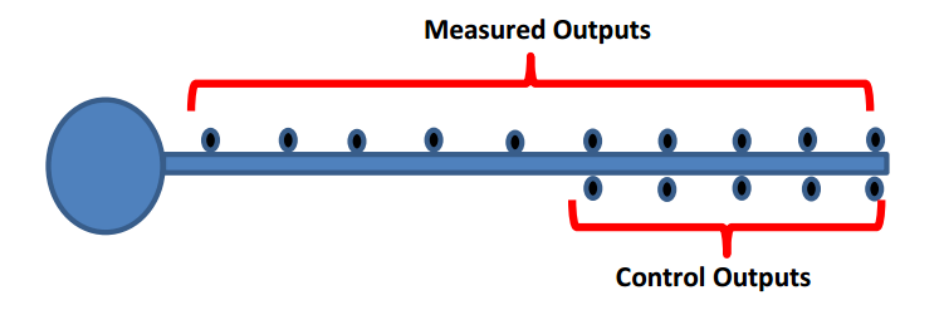


Figure 3.1. Locations of Measured and Control Outputs

3.2 Model Reduction

To use MCA (described in Chapter 2), the model in Equation (3.10) is transformed into modal coordinates using a transformation matrix T. The system matrices are then described by

$$\hat{A} = (T)^{-1}A(T) \tag{3.11a}$$

$$\hat{B} = (T)^{-1}B \tag{3.11b}$$

$$\hat{C} = C(T) \tag{3.11c}$$

$$\widehat{M} = M(T) \tag{3.11d}$$

$$\widehat{D} = (T)^{-1}D \tag{3.11e}$$

with \hat{A} block diagonal – the first 3x3 block corresponding to turbulence, the next 2x2 block corresponding to the rigid body mode, and lastly the 20 aeroelastic modes. So, for the simplified model, the first 5x5 block was removed.

The algorithm described in Chapter 2 was used to perform MCA on the full-order model in Equation (3.10) in modal coordinates. The weighting matrix Q was chosen to be equal to the identity matrix. 6 modes with the highest modal costs were kept, producing a 12^{th} order reduced-order model, which will be referred to as the design model:

$$\dot{x} = A_d x + B_d u + D_d w \tag{3.12a}$$

$$y = C_d x \tag{3.12b}$$

$$z = M_d x + v . (3.12c)$$

Table 3.1 below gives the modal costs of the evaluation model [21].

Table 3.1. Modal Cost Analysis

index	Modal costs	Mode number
	(% normalized)	
1	1.3240e-003	7
2	8.8672e-003	8
3	2.7167e-002	11
4	3.7154e-002	14
5	6.3904e-002	13
6	3.3843e-001	12
7	3.4204e-001	15
8	3.6106e-001	9
9	4.8207e-001	16
10	5.2073e-001	10
11	7.3007e-001	17
12	1.1763e+000	18
13	3.0376e+000	19
14	3.1012e+000	20
15	5.6577e+000	5
16	7.4217e+000	6
17	8.6460e+000	2
18	1.3342e+001	1
19	2.0328e+001	3
20	3.4376e+001	4

Figures 3.2a and 3.2b show a comparison of the impulse responses from the sixth input to the fourth output and from the fourth input to the fifth output, respectively. The plots show that the responses after model reduction vary only slightly in the first half second, and are nearly identical afterward. Therefore, the 12th order design model is a good lower-order representation of the full-order evaluation model.

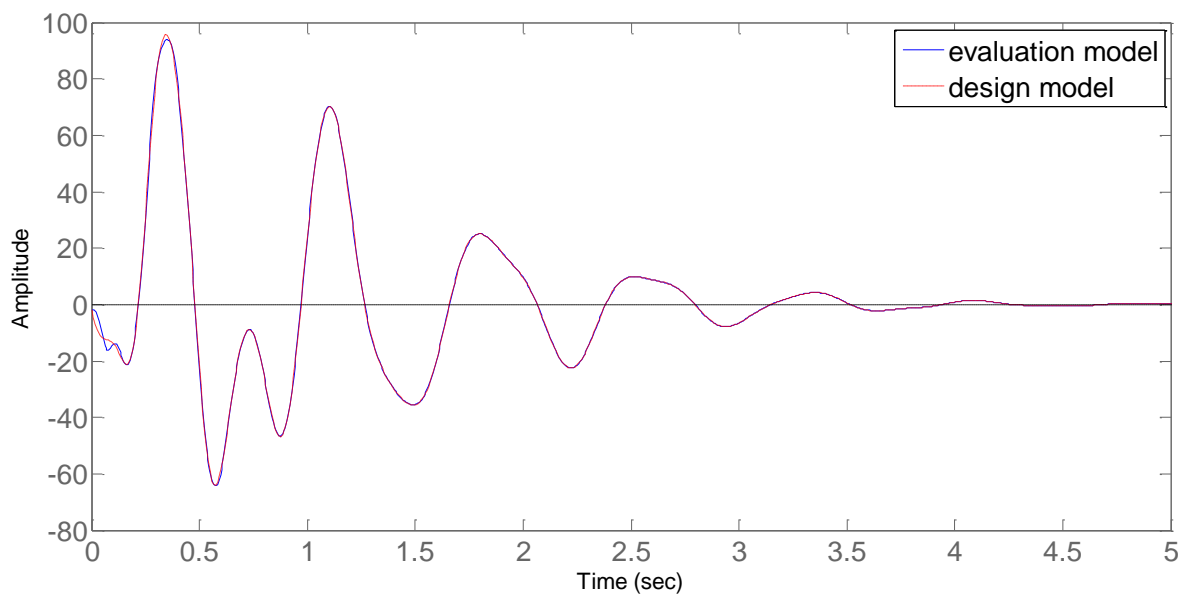


Figure 3.2a. Impulse Response of Evaluation and Design Models: 6^{th} Input to 4^{th} Output

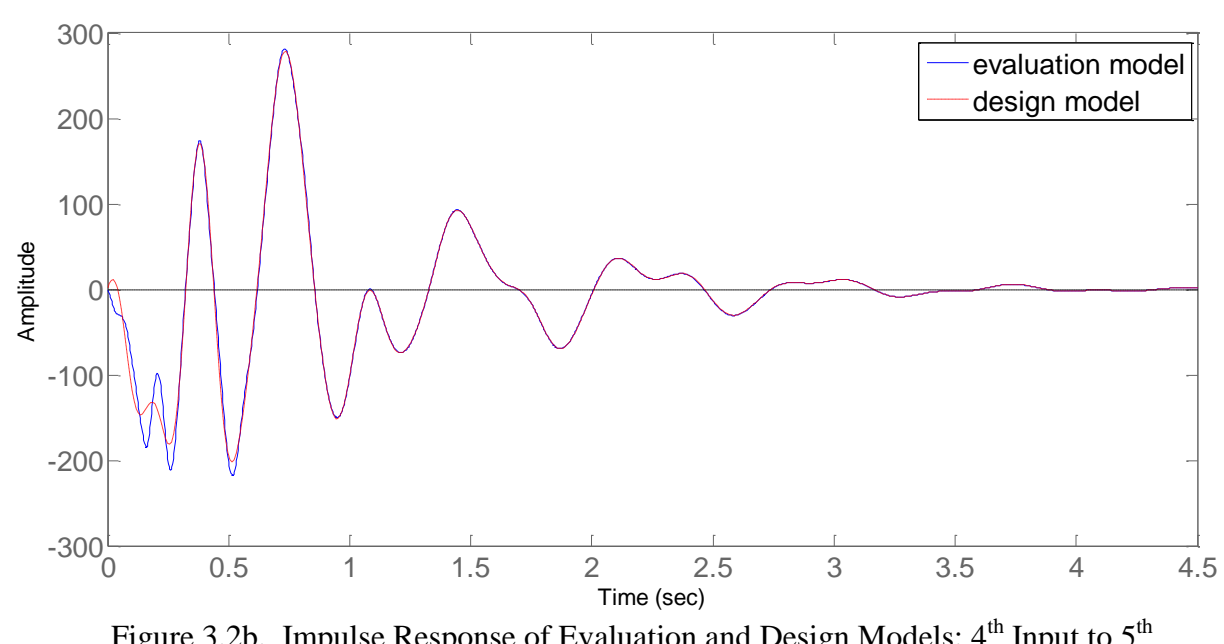


Figure 3.2b. Impulse Response of Evaluation and Design Models: 4^{th} Input to 5^{th} Output

3.3 Simulation Study

3.3.1 Simulation Set-up

The evaluation model described in Section 3.1 and the design model described in 3.2 was input into a MATLAB script that performed the OCC algorithm (given in the Appendix). First,

the variables that do not depend on the weighting matrix Q, F and \tilde{X} from Equations (2.11c and 2.11e), were calculated. The program includes two loops: the outer loop iterates on the output covariance constraint \bar{Y}^b , which is decreased, and an inner loop that corresponds to the OCC algorithm presented in Section 2.1.2.

At the beginning of the outer loop, \bar{Y}^b is calculated based on the following equation:

$$\bar{Y}^b = I_{12} \cdot norm(\gamma \cdot \bar{Y}_{0L}) + block \ diag[Y_{d,1}, Y_{d,2}, \dots, Y_{d,m}], \tag{3.13}$$

where $Y_{d,i} = C_{d,i} \tilde{X} C_{d,i}^T$ (i = 1, 2, ..., m), γ is initially 0.95 and is decreased by 0.05 each iteration of the outer loop, and \bar{Y}_{OL} is solved from the following equation:

$$\bar{Y}_{OL} = block \ diag[\bar{Y}_{OL1}, \bar{Y}_{OL2}, \dots, \bar{Y}_{OLm}], \tag{3.14}$$

where $\bar{Y}_{OL,i} = (C_{d,i}X_{OL}C_{d,i}^T)$ (i = 1, 2, ..., m) and X_{OL} is solved by

$$0 = AX_{OL} + X_{OL}A^{T} + DW_{p}D^{T}. (3.15)$$

This loop continues as long as γ is above 0. The purpose of this loop is to find a sequence of OCC controllers with control effort from low to high.

The inner loop goes through the OCC algorithm, calculating K, G, X, and Y^b . For each inner loop iteration, the convergence condition given in Step 3 of the OCC algorithm is tested with ε chosen as 10^{-6} . If it fails, a new Q is calculated according to the equation for Q(i+1) in Step 5. For this model, the values $\alpha=0.2$ and $\beta=0.8$ were used, resulting in convergence for all \overline{Y}^b conditions besides the last one corresponding to $\gamma=0.05$. Then, the inner loop continues with this updated Q value. If the condition in Step 3 passes (convergence), then the inner loop is exited.

The block diagonal matrix consisting of the output variances for the evaluation model is then computed:

$$Y_e = block \ diag[Y_{e,1}, Y_{e,2}, ..., Y_{e,m}],$$
 (3.16)

where $Y_{e,i} = C_{CL,i}X_{CL}C_{CL,i}^T$ (i = 1, 2, ..., m), $C_{CL} = [C \ 0_{12}]$, and the closed-loop state X_{CL} is the solution to

$$0 = A_{CL}X_{CL} + X_{CL}A_{CL}^{T} + D_{CL}\overline{W}D_{CL}^{T}, (3.17)$$

where

$$\overline{W} = diag(W_p, V) \tag{3.18}$$

and A_{CL} and D_{CL} following from Equation (2.5) in Chapter 2 as:

$$A_{CL} = \begin{bmatrix} A & BG \\ FM & A_C \end{bmatrix}, \tag{3.19}$$

where

$$A_c = A_d + B_d G - F M_d \tag{3.20a}$$

$$D_{CL} = \begin{bmatrix} D & 0_{40x42} \\ 0_{12x1} & F \end{bmatrix}. \tag{3.20b}$$

For plotting the results, the input covariance U_{CL} , which corresponds to the control energy, is also calculated:

$$U_{CL} = C_{u,CL} X_{CL} C_{u,CL}^{T}, (3.21)$$

where $C_{u,CL} = [0_{13x40} \ G]$ and G is the value from the last iteration of the inner loop. At the end of the outer loop, γ is decremented, and the loop iterates, with the last iteration at $\gamma = 0.05$.

3.3.2 Simulation Results

The following two plots were generated by the MATLAB program described in Section 3.3.1. Figure 3.3 shows the output variances with respect to the design model and the output variances with respect to the evaluation model, against iteration of the outer loop. The 18 iterations that converged are included (excluding when $\gamma = 0.05$), and the 18 points each correspond to a designed controller. The design model is plotted with a solid line and the evaluation model in a dashed line. However, the overlap of the design and evaluation model

variances in most of the plot results in the appearance of only the design model being plotted. The variances of each of the 10 outputs are plotted separately. Therefore, the plot includes 20 lines, 10 with respect to each of the models. Only 5 outputs can be easily seen however, because the remaining ones are much closer to 0.

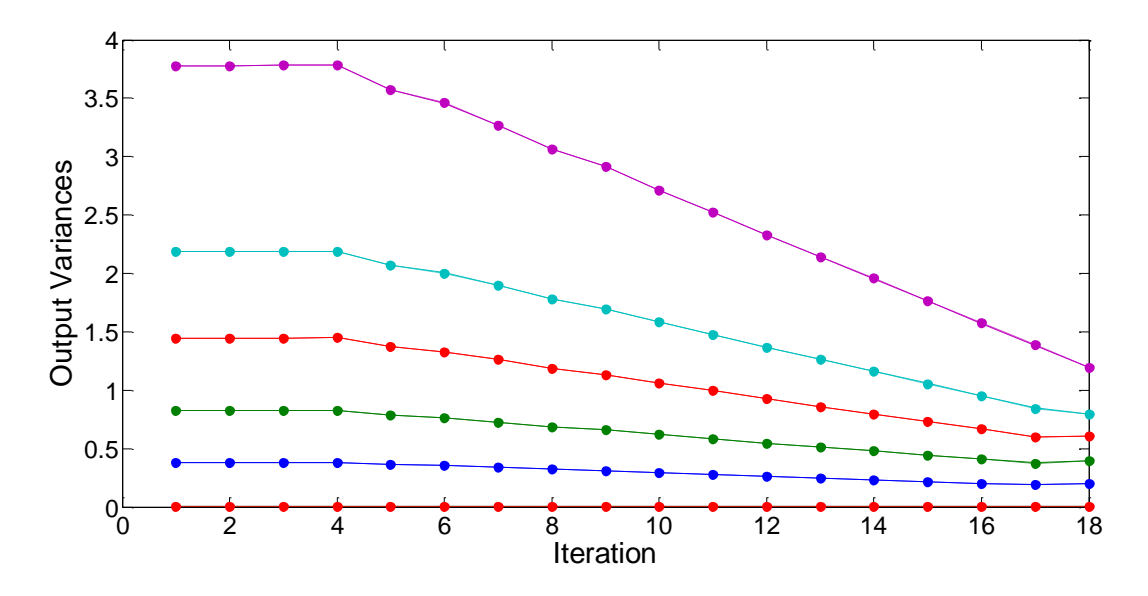


Figure 3.3. Output Variances vs. Iteration Number

Figure 3.4 shows the same output variances, but plotted against the input covariance, described in Equation (3.21). Again, each point corresponds to a controller designed for a given output covariance constraint. The shape of the plot and the spacing of the points reveal the tradeoff between output variance and control energy used to achieve that output variance. As output variance of each output decreases, input covariance increases. This means that as performance increases, control energy increases, and at a faster rate. The ideal controller would then be chosen by considering the desired performance and level of control, with the best controller generally corresponding to one of the points in the lower left side of the plot (lower output variance and input covariance).

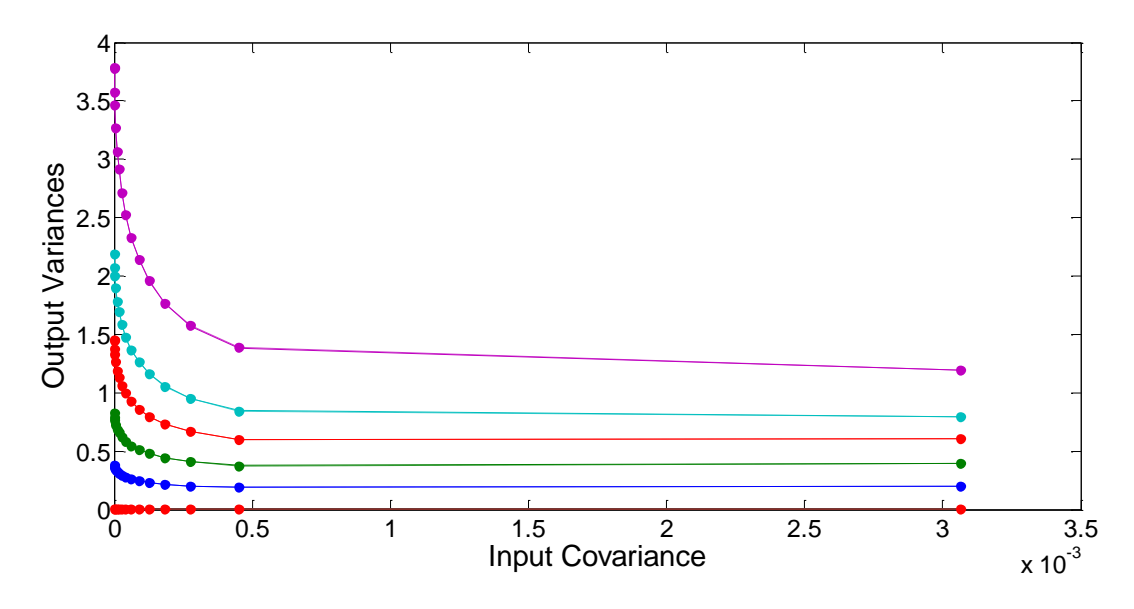


Figure 3.4. Output Variances vs. Input Covariance

Figures 3.5a and 3.5b show a comparison of the open-loop and closed-loop impulse response from the 16th iteration of the outer loop of the controller design. This controller was chosen based on a reasonable tradeoff between performance and control energy. The response is from the wind gust input to the fifth and seventh outputs, respectively. The plots verify that the designed controller reduces the amplitude of the aeroelastic modes to nearly zero, such that the amplitude cannot easily be seen on the plot, compared to the much larger open loop response.

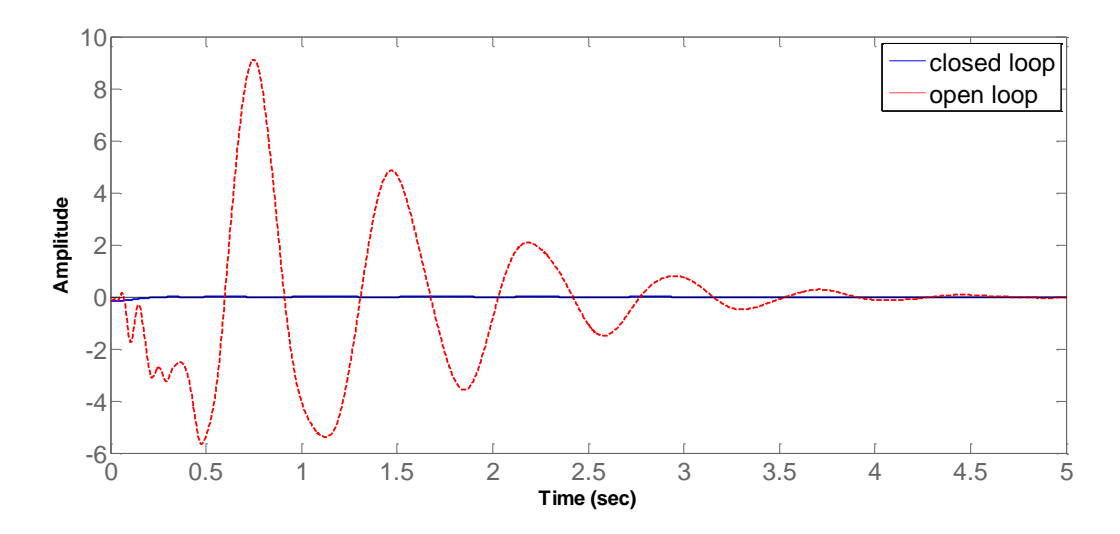


Figure 3.5a. Impulse Response of the Open and Closed-Loop Systems from Wind Input to $5^{\rm th}$ Output

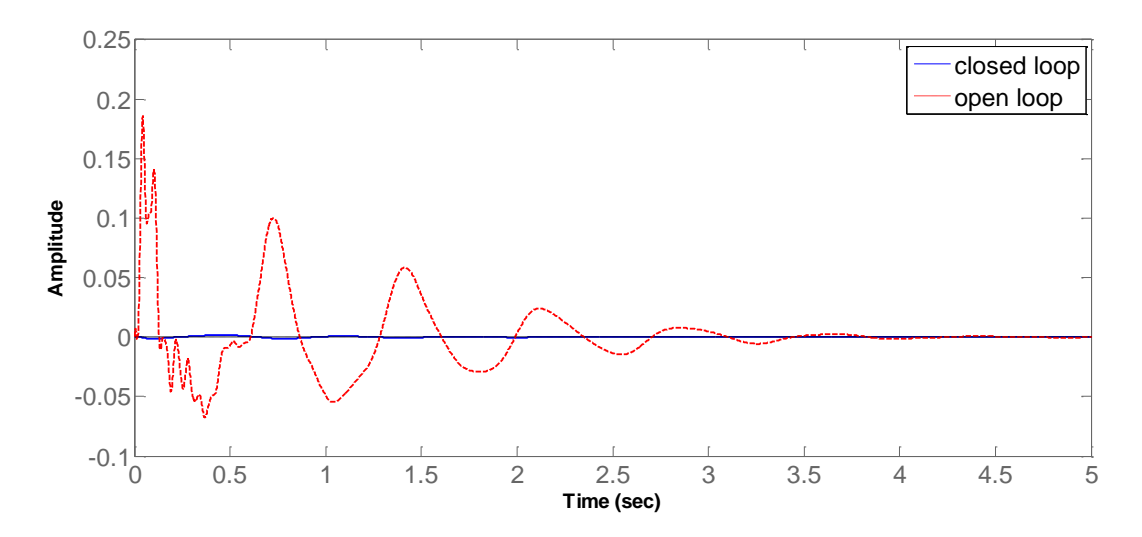


Figure 3.5b. Impulse Response of the Open and Closed-Loop Systems from Wind Input to 7th Output

Figures 3.6a and 3.6b show the bending displacements of each measured point on the wing for the open and closed-loop situations, respectively. The controller used in the closed-loop case is again that from the 16th iteration of the outer loop of the controller design (also used in Section 3.3.3 for the next round of MCA and OCC). If Figure 3.1 corresponds to the side view of the wing with no forces applied, the following plots show the shape of the wing for 3 time steps to an impulse response on the wind input. As in Figure 3.1, the rightmost point corresponds to that of the wing tip, and the 5 rightmost points are the control outputs. The lines in Figure 3.6b are nearly horizontal on the same scale, showing that the bending vibrations have been significantly reduced.

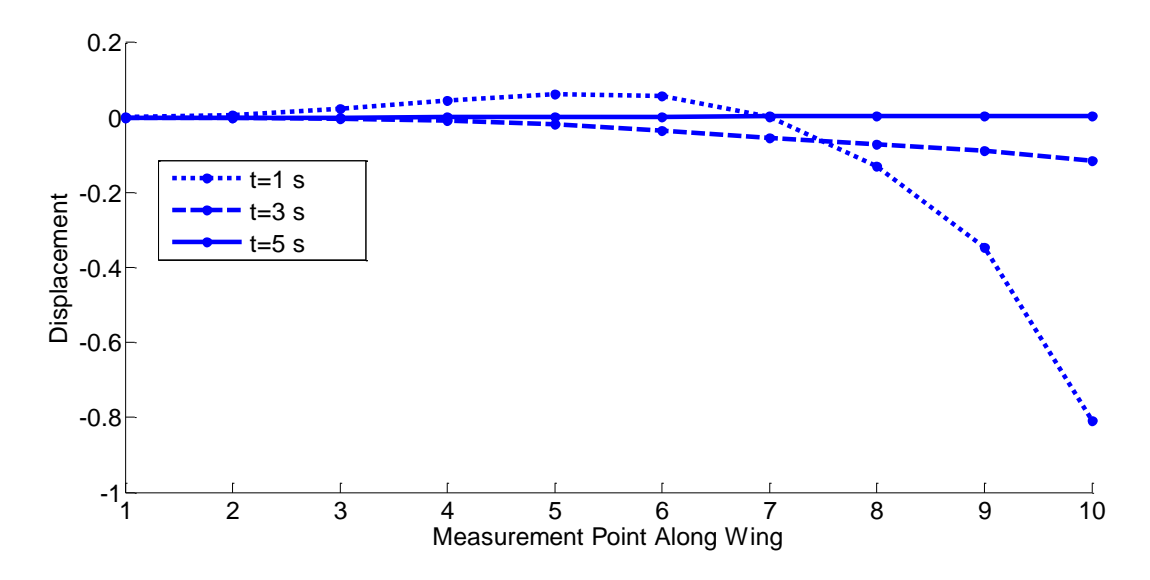


Figure 3.6a. Open-Loop Wing Deformation with Time

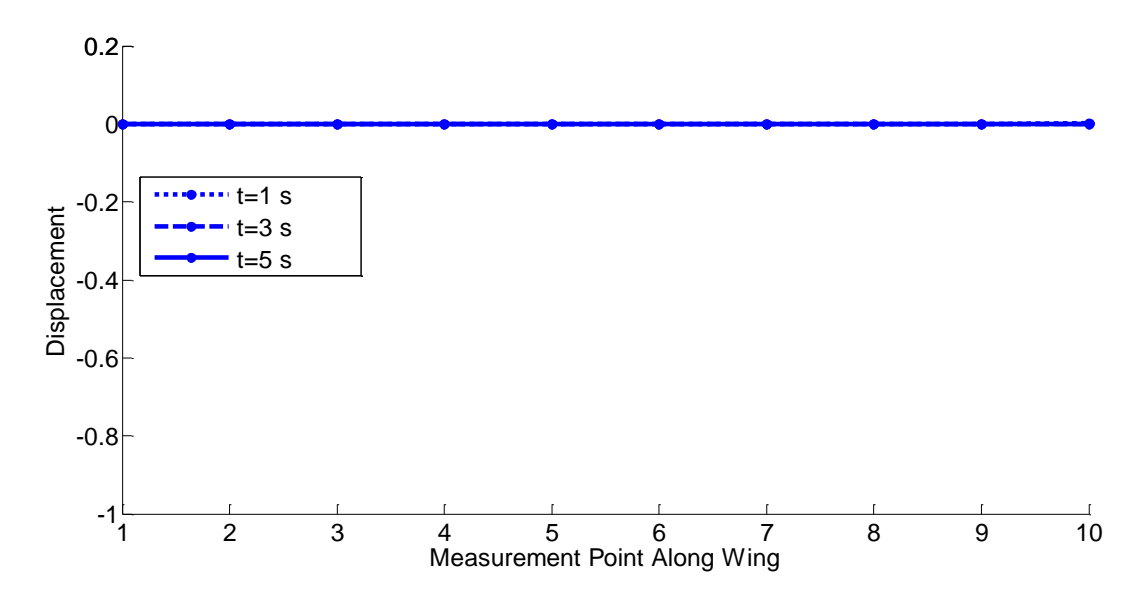


Figure 3.6b. Closed-Loop Wing Deformation with Time

3.3.3 Iteration on OCC and MCA

In the previous section, an optimal controller was found for the 12th order design model, and was shown to significantly reduce the amplitude of the impulse response with the evaluation model. The next step was to iterate once again on the model reduction algorithm and controller design to achieve a similar performance output with a lower-order controller. The goal of this section is to describe the iteration process and show the results of the second simulation.

18 weighting matrices, Q_i , were found after completing the OCC algorithm described in Section 3.3.1. As discussed in the last section, one of the latter Q values, that from the 16^{th} controller, was chosen. As mentioned in Section 2.2, this Q relates to the most significant modes of the system. Therefore, a modified version of this Q was used in the second round of model reduction, which will be referred to as Q Loop 1 (Q Loop 0 is the initial model reduction and controller design. See Figure 2.1). In order to capture the effect of the new Q, it was multiplied by a large scalar (specifically, 10^8), so that the effect of the 10 control outputs could be seen over the weighting of the measured outputs, which remained unchanged in the second iteration of MCA (Q Loop 1). Using this scaled Q value, the same 6 modes had the highest modal costs. However, the scaling shows that the relative difference between the 4 highest-cost modes and the two immediately lower ones increased. This indicates that the new Q value further allowed the model to be reduced to its 4 most significant modes, resulting in an 8^{th} order system. The results of MCA are shown below in Table 3.2. The table shows the larger difference between modes 5 and 6 as compared to 2, 4, 3, and 1.

Table 3.2 Modal Cost Analysis for Q Loop 1

index	Modal costs	Mode number
	(% normalized)	
1	7.2915e-006	7
2	4.4933e-005	8
3	2.1286e-004	11
4	3.8955e-004	14
5	4.5625e-004	13
6	1.8486e-003	12
7	1.8572e-003	9
8	1.9948e-003	15
9	2.6692e-003	10
10	6.1122e-003	16
11	1.2153e-002	17
12	5.0192e-002	18
13	1.4500e-001	19
14	2.5058e-001	20
15	1.0227e+000	5
16	1.5383e+000	6
17	1.5351e+001	2
18	2.5339e+001	4
19	2.6802e+001	3
20	2.9473e+001	1

Again, two impulse responses were plotted, as in Figures 3.2a and 3.2b, this time to compare the evaluation model to the 8th order reduced model. The result is plotted in Figures 3.7a and 3.7b, and shows the validity of this further reduced model.

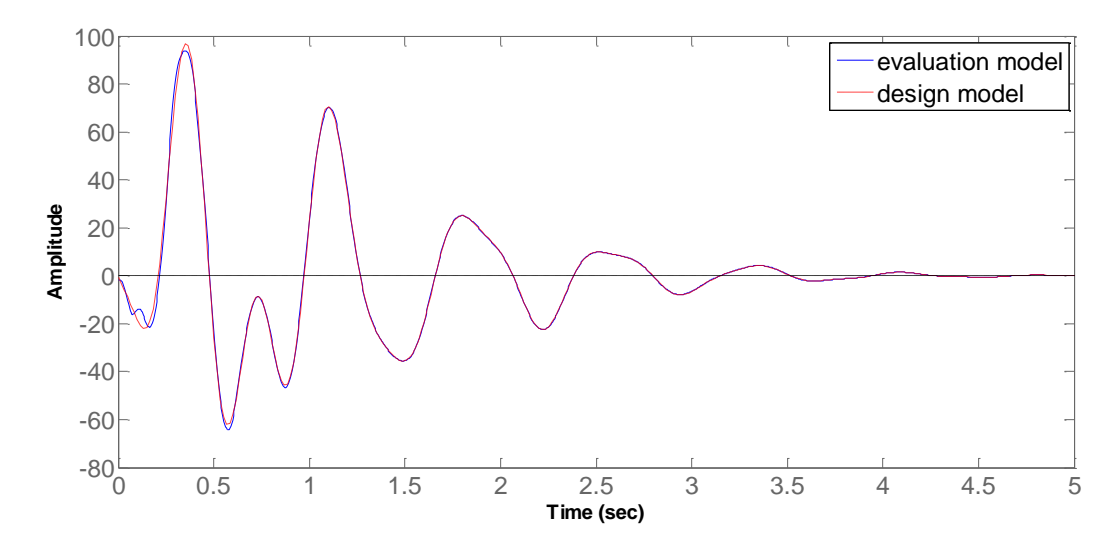


Figure 3.7a. Impulse Response of Evaluation and 8^{th} Order Design Models: 6^{th} Input to 4^{th} Output

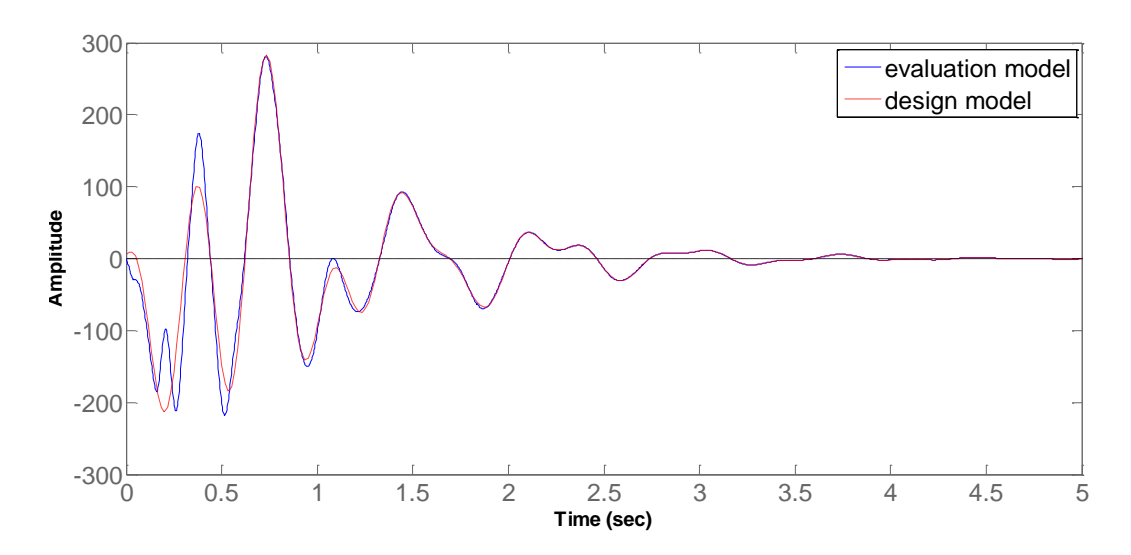


Figure 3.7b. Impulse Response of Evaluation and 8^{th} Order Design Models: 4^{th} Input to 5^{th} Output

The OCC algorithm was then run using the original evaluation model and the new design model. Instead of beginning the algorithm with Q equal to identity, the Q value that was found before scaling for the model reduction was used to start. The same plots as in the first Q loop were produced, which are shown below in Figures 3.8a and 3.8b. The dashed lines correspond to the evaluation model. The plots show that the output variance values decrease as before. Additionally, for all but the topmost output, the variance values are below or very close to those in the first OCC iteration, Q Loop 0.

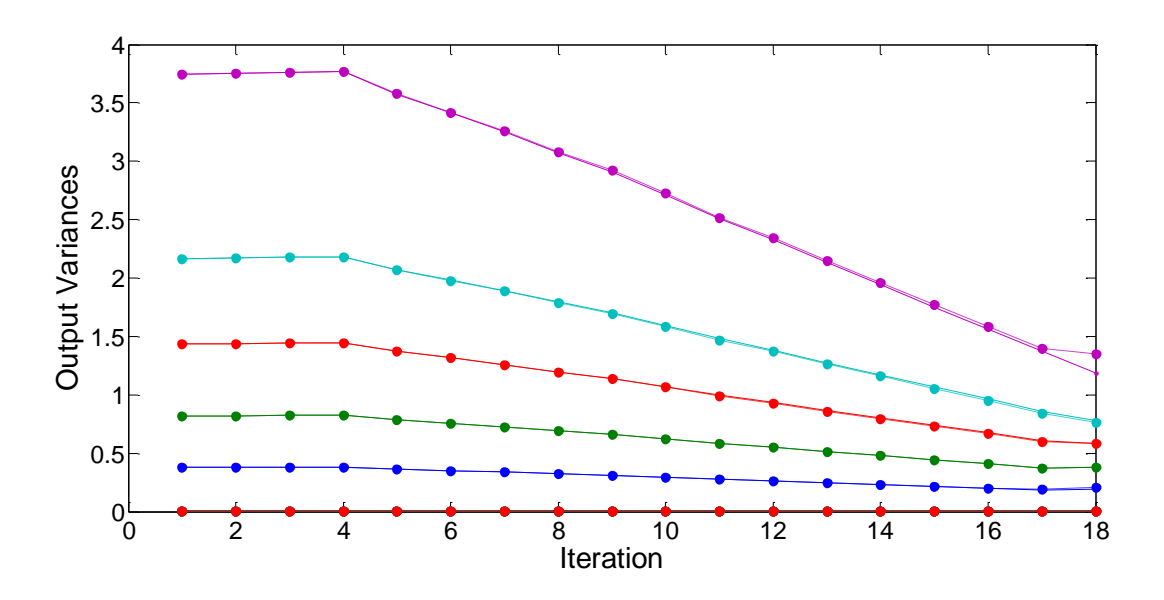


Figure 3.8a. Output Variances vs. Iteration Number for Q Loop 1

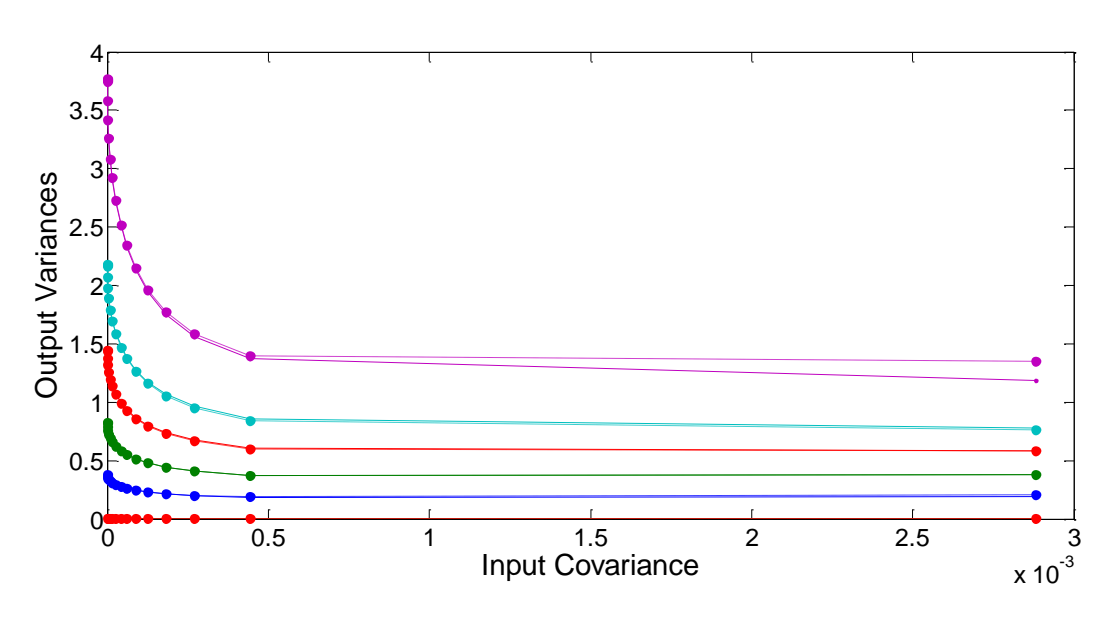


Figure 3.8b. Output Variances vs. Input Covariance for Q Loop 1

Lastly, Figures 3.9a and 3.9b show the open-loop vs. closed-loop responses made again with the 16^{th} controller of Q Loop 1. The plots show that the vibrations are once again reduced significantly.

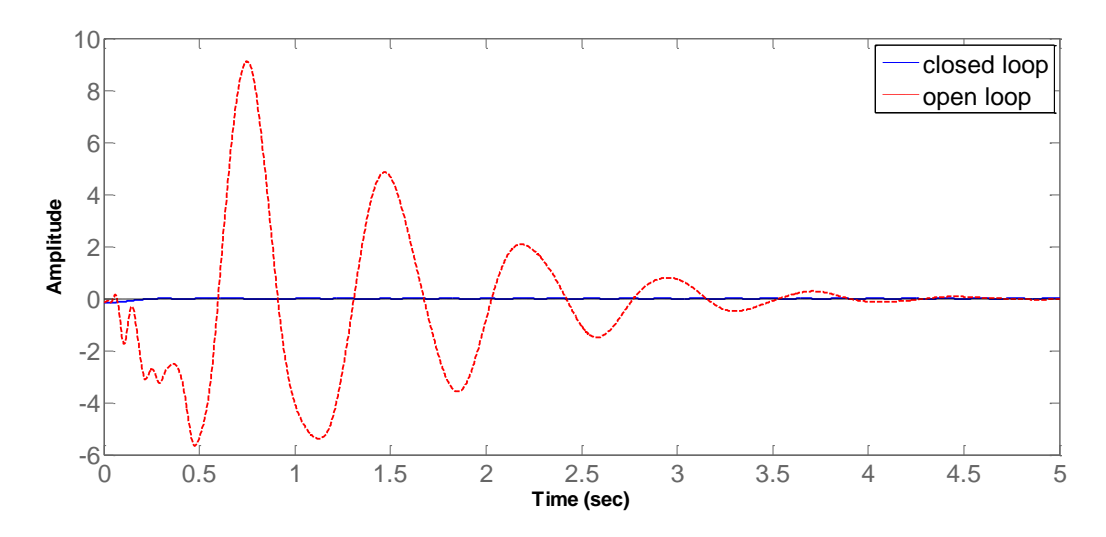


Figure 3.9a. Open vs. Closed-Loop Impulse Response of Wind to 5^{th} Output for Q Loop 1

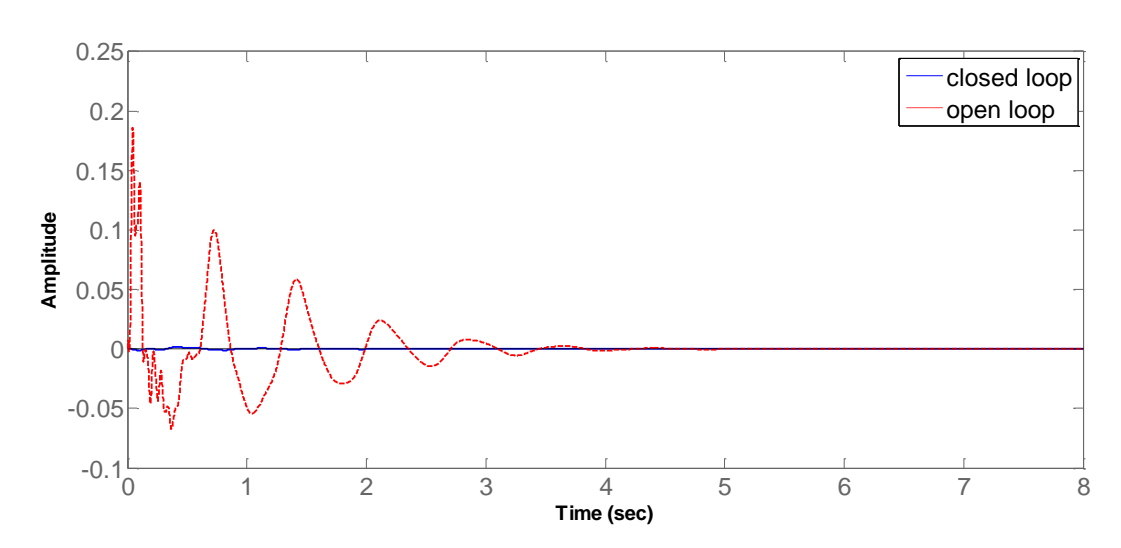
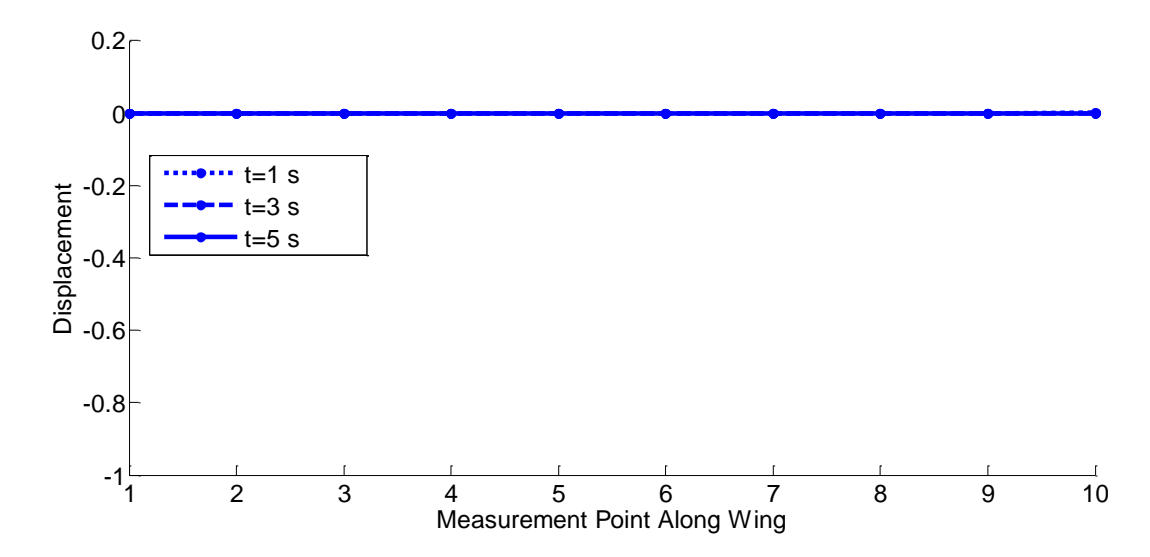


Figure 3.9b. Open vs. Closed-Loop Impulse Response of Wind to 7^{th} Output for Q Loop 1

Figure 3.10 corresponds to Figure 3.6b, and shows the bending displacement of the whole wing at 3 time points using the 16th controller designed in Q Loop 1. By comparing to the open-loop plot in Figure 3.6a, it can be seen that the bending displacements are reduced equally effectively using the lower-order 8th order controller as with the 12th order controller from Q Loop 0.



3.10. Closed-Loop Wing Deformation with Time for Q Loop 1

CHAPTER 4: CONCLUSION

In this work, control for vibration reduction is applied to modern, elastic aircraft wings. With increased structural flexibility comes a greater interaction with aerodynamic forces, which increases the need and challenge for an effective controller design. The aircraft physical system is often very high-order and must be reduced. This work presented an integrated controller design and model reduction method to realize the natural coupling of the two steps. MCA was used to first reduce the order of the model to a certain level that would allow a practical controller to be designed and implemented. After that, the OCC control design algorithm was implemented to produce a controller for the reduced-order model, which was verified for the full-order model. A second iteration on the model reduction and controller design process used the weighting matrix found in the first iteration to show that an even lower-order model can be used in the OCC algorithm, and a new controller was again verified for the full-order model.

Using plots of the variance values of the bending displacement and rates outputs, as well as a comparison between open and closed-loop impulse responses to a random wind input, it was shown that the controllers designed in both Q-loop iterations were successful in significantly reducing wing vibrations, with the lower-order controller performing equally effectively.

APPENDIX

OCC PROGRAM CODE

```
% load design model
['load cdmodel ' int2str(Q loop) '.mat'];
eval(ans);
% load evaluation model
load cemodel 0.mat
% load some parameters
if Q loop==0
    load weight.mat
    ['load weight' int2str(Q loop) '.mat'];
    eval(ans);
end
% for subsequent Q loop iterations
if Q loop>0
    Q=Qred; % Q is that from the last Q loop iteration
end
% define more parameters
epsi = 1*10^-6;
Beta = 0.8; % 0<Beta<1</pre>
alpha = .2; % alpha>0
gamma = 0.95;
count = 1; % gamma iteration
N = 500;
num iter(1:19)=0;
Q1 = Q;
% ititialize to 0
Yd i = zeros(10,19);
Ye i = zeros(10,19);
Yd_norm = zeros(1,18);
Ye norm = zeros(1,18);
[sr,sc]=size(EMd0);
[X tilde, L, G] =
care(EAd0',EMd0',EDd0*W*EDd0',V,zeros(sc,40),eye(length(EAd0)));
F = X tilde*EMd0'/(V);
X OL = lyap(EAd0, EDd0*W*EDd0');
Yb OL=diag(diag(ECd0*X OL*ECd0'));
while gamma >= 0
```

```
Yb bar = eye(10)*norm(gamma*Yb OL) + diag(diag(ECd0*X tilde*ECd0'));
      recalculate Q with new Yb bar (after initial iteration when we start
with O=I
    if count ~= 1
       M = Q + alpha*(Yb-Yb bar);
          Schur decomposition on M:
        [U,T] = schur(M);
        % then make negative diag == 0
        for k=1:10
            if T(k, k) < 0
                T(k, k) = 0;
            end
        end
        P = U*T*U';
        Q = Beta*Q+(1-Beta)*P;
        eval(['Q' int2str(count) '=Q;']);
    end
    for j=1:N % however long you want to allow to converge (get below
        num iter(count) = num iter(count)+1;
        % for each changing Q:
        [sr,sc]=size(EBd0);
        [K,blah,blahh] =
care(EAd0,EBd0,ECd0'*Q*ECd0,R,zeros(sr,13),eye(length(EAd0)));
        G = -inv(R) *EBd0'*K;
        X = lyap(EAd0+EBd0*G,F*V*F');
        % for design model
        Yb = diag(diag(ECd0*(X tilde+X)*ECd0'));
        test = norm((Yb-Yb bar)*Q);
        if test < epsi</pre>
            disp(['Converged after ', num2str(num iter(count)), ' iterations
when gamma = ', num2str(gamma)]);
           break % BREAK 1
        elseif j==N
            disp(['Did not converge for gamma = ', num2str(gamma)]);
            break % BREAK 1
        end
        % Else update Q
        M = Q + alpha*(Yb-Yb bar);
        % Schur decomposition on M:
        [U,T] = schur(M);
        % then make negative diag == 0
        for k=1:10
            if T(k,k) < 0
                T(k, k) = 0;
            end
        end
```

```
P = U*T*U';
        Q = Beta*Q+(1-Beta)*P;
        Qnorm(j,count) = norm(Q); % supposed to go up
        eval(['Q' int2str(count) '=Q;']); % could be outside loop
    end
        BREAK 1 goes to here
       For design model
    Yd i(:,count) = diag(ECd0*(X tilde+X)*ECd0'); % gives column vector
    Yd norm(count) = norm(diag(diag(ECd0*(X tilde+X)*ECd0')));
    % For evaluation model
    % Output Covariance Ye for evaluation model
    Ac = EAd0+EBd0*G-F*EMd0;
    A CL = [EA0 EB0*G ; F*EM0 Ac];
    [sr,sc]=size(ECd0);
    C CL = [EC0 zeros(10,sc)];
    D CL = [ED0 zeros(length(ED0), 40) ; zeros(length(EAd0), 1) F];
    W \text{ bar} = [W \text{ zeros}(1,40) ; \text{ zeros}(40,1) V];
    Xe_CL = lyap(A_CL,D_CL*W_bar*D_CL');
      Save every closed-loop system
    ['save CLsys' int2str(Q loop) ' ' int2str(count) ' A CL C CL D CL'];
    eval(ans);
    % Input Covariance U_CL
    Cu CL = [zeros(13, length(EA0)) G];
    U_CL = Cu_CL*Xe_CL*Cu_CL';
    U_CL_plot(count) = trace(U_CL);
    Ye i(:,count) = diag(C CL*(Xe CL)*C CL'); % gives column vector
    Ye norm(count) = norm(diag(diag(C CL*(Xe CL)*C CL')));
    gamma = gamma - 0.05;
    count = count+1; % gamma changes
% Plot results
figure
plot(Yd i(:,1:(end-1))','.-')
hold on
plot(Ye i(:,1:(end-1))','--.')
xlabel('Iteration')
ylabel('Output Variances')
figure
plot(U CL plot(1:(end-1)), Yd i(:,1:(end-1))','.-')
hold on
plot(U CL plot(1:(end-1)), Ye i(:,1:(end-1))','--.')
xlabel('Input Covariance')
ylabel('Output Variances')
```

end

BIBLIOGRAPHY

BIBLIOGRAPHY

- [1] C. Moutinho, A. Cunha, and E. Caetano, "Implementation of active and passive control systems in laboratorial and real structures," *S3T*, 2010.
- [2] K. M. Grigoriadis, G. Zhu, and R. E. Skelton, "Optimal Redesign of Linear Systems," *J. Dyn. Syst. Meas. Control*, vol. 118, no. 3, pp. 598–605, Sep. 1996.
- [3] J. Q. Sun, M. R. Jolly, and M. A. Norris, "Passive, Adaptive and Active Tuned Vibration Absorbers—A Survey," *J. Mech. Des.*, vol. 117, no. B, pp. 234–242, Jun. 1995.
- [4] P. Gardonio, "Review of Active Techniques for Aerospace Vibro-Acoustic Control," *J. Aircr.*, vol. 39, no. 2, pp. 206–214, Apr. 2002.
- [5] K. Adachi, K. Sakamoto, and T. Iwatsubo, "Redesign of closed loop system for integrated design of structure and its vibration control system," in *Proceedings of the 1999 IEEE International Conference on Control Applications, 1999*, 1999, vol. 1, pp. 80–85 vol. 1.
- [6] E. Gildin, "Model and controller reduction of large-scale structures based on projection methods," The University of Texas at Austin, Austin, Texas, 2006.
- [7] T. T. Soong and B. F. Spencer Jr, "ACTIVE, SEMI-ACTIVE AND HYBRID CONTROL OF STRUCTURES," in *Proceedings of the Twelfth World Conference on Earthquake Engineering*, Auckland, New Zealand, 2000.
- [8] B. J. Grobbelaar, G. D. Wood, and C. P. Constancon, "Application of Modal Control to Flexible Structures," *NO J.*, pp. 18–24, Jul. 1992.
- [9] "Active Control of Flexible 2020 Aircraft Transport Research & Innovation European Commission," *European Commission*. [Online]. Available: http://ec.europa.eu/research/transport/projects/items/acfa_2020_en.htm. [Accessed: 13-Jul-2014].
- [10] C. M. D. Wilson and M. M. Abdullah, "Structural Vibration Reduction Using Fuzzy Control of Magnetorheological Dampers," in *Structures Congress* 2005, American Society of Civil Engineers, pp. 1–12.
- [11] S. S.-M. Swei, G. G. Zhu, and N. T. Nguyen, "Integrated Model Reduction and Control of Aircraft with Flexible Wings," presented at the AIAA Guidance, Navigation, and Control (GNC) Conference, Boston, MA.
- [12] J. M. Barker, G. J. Balas, and P. . Blue, "Active flutter suppression via gain-scheduled linear fractional control," in *American Control Conference*, 1999. Proceedings of the 1999, 1999, vol. 6, pp. 4014–4018 vol.6.
- [13] P. Haley and D. Soloway, "Generalized predictive control for active flutter suppression," *IEEE Control Syst.*, vol. 17, no. 4, pp. 64–70, Aug. 1997.

- [14] J. H. Kim, "Model reduction, sensor/actuator selection and control system redesign for large flexible structures," Ph.D., Purdue University, United States -- Indiana, 1991.
- [15] G. Zhu, K. M. Grigoriadis, and R. E. Skelton, "Covariance Control Design for Hubble Space Telescope," *J. Guid. Control Dyn.*, vol. 18, no. 2, pp. 230–236, Apr. 1995.
- [16] G. Zhu and R. E. Skelton, "Integrated Modeling and Control for the Large Spacecraft Control Laboratory Experiment Facility," *J. Guid. Control Dyn.*, vol. 17, no. 3, pp. 442–450, Jun. 1994.
- [17] A. C. Antoulasr and D. C. Sorensen, "Approximation of large-scale dynamical systems: An overview," 2001.
- [18] N. Nguyen and J. Urnes, "Aeroelastic Modeling of Elastically Shaped Aircraft Concept via Wing Shaping Control for Drag Reduction," in *AIAA Atmospheric Flight Mechanics Conference*, American Institute of Aeronautics and Astronautics.
- [19] G. Zhu, M. A. Rotea, and R. Skelton, "A convergent algorithm for the output covariance constraint control problem," *SIAM J. Control Optim.*, vol. 35, no. 1, pp. 341–361, 1997.
- [20] G. Zhu, "L_2 AND L_INFINITY MULTIOBJECTIVE CONTROL FOR LINEAR SYSTEMS," Purdue University, West Lafayette, IN, 1992.
- [21] G. Zhu and R. E. Skelton, "INTEGRATED MODELING AND CONTROL SOFTWARE," Dynamic Systems Research, INC, West Lafayette, IN, Sep. 1992.